Ocean Engineering 357 (2026) 125487

Contents lists available at ScienceDirect

Ocean Engineering

journal homepage: www.elsevier.com/locate/oceaneng

Research paper

Dependence models and Gamma process for single-defect deterioration of a rock-armored groyne under ship-wave attack

Patricia Mares-Nasarre [a,*], Gregor Melling [b], Oswaldo Morales-Nápoles [a]

[a] Faculty of Civil Engineering and Geosciences, Delft University of Technology, Delft, The Netherlands
[b] Federal Waterways Engineering and Research Institute (BAW), Hamburg, Germany

ARTICLE INFO

Keywords:
Armor damage
Rock groynes
Ship waves
Structure deterioration
Gamma process
Multivariate distribution

ABSTRACT

Infrastructures are facing growing challenges due to their aging process while climate change and evolution of traffic and shipping fleets are increasing the uncertainty of loadings in the future. This study proposes a method to assess the survivability of structures with gradual deterioration under changing loading scenarios based on field data. The methodology is applied to the armor deterioration of a rock-armored groyne under ship-wave attack. First, we generate synthetic timeseries of damage by coupling a Poisson distribution to determine the number of passing ships per day, a vine-copula to quantify the multivariate joint distribution of the loading variables that define the primary wave height and a Bernoulli process and a bivariate copula to translate the primary wave height into the increment of damage. Afterwards, these damage curves are used to quantify a Gamma process. Thus, it is possible to conditionalize the joint distribution of the loading variables to generate the damage curves under different loading scenarios and evaluate the effects of these scenarios on the structure's survivability. We exemplify the use of the methodology to assess the armor deterioration of a rock-armored groyne under ship-wave attack with and without a limitation in the speed velocity in the waterway.

1. Introduction

Aging infrastructures face growing challenges as they deteriorate over time (ASCE, 2021). In sectors such as waterborne transportation and coastal engineering, rising sea levels and stronger wave storms caused by climate change (Camus et al., 2019) and the continuous evolution of shipping fleets and traffic patterns (Haralambides, 2017) introduce heightened uncertainty about the future loads these structures will encounter. In response to these challenges, methodologies to assess the survivability of structures under different loading scenarios are necessary to better plan maintenance, repair, or upgrade of existing structures.

To define a methodology to assess the survivability of infrastructures under different loading scenarios, two aspects need to be addressed: (1) generation of synthetic timeseries of deterioration under different loading scenarios, and (2) modeling the deterioration of the structure over time. The generation of the aforementioned synthetic timeseries requires both the loadings and the response of the structure to be modeled. To model the loading, typically the joint distribution of several random variables is quantified. Some approaches assume the independence between the different variables used to characterize the loading (e.g. Pugh and Vassie, 1978), although they are generally generated by the same drivers and, thus, they are dependent (e.g. Mares-Nasarre et al., 2023; Noh and Sun, 2025). Consequently, authors in literature have proposed different probabilistic models to quantify the joint multivariate distribution of the loading variables. Bivariate copulas have been widely applied when the loading can be modeled using only two random variables (e.g. wind speed and significant wave height in Noh and Sun, 2025). However, more than two variables are often required to accurately describe the loading. In those cases, copula-based methods such as Gaussian copula-based Bayesian Networks (GCBN) or vine-copulas are gaining popularity (e.g. Mares-Nasarre et al., 2024b; Zhao and Dong, 2025). One of the main differences between GCBN and vine-copulas is that GCBNs model the dependence of the variables using Gaussian copulas and, thus, they do not account for asymmetries in the dependence structure. On the contrary, vine-copulas are highly flexible models that allow to build the joint distribution in bivariate pieces using different copulas. For this reason, the use of vine-copulas is rapidly increasing in literature (e.g. Mares-Nasarre et al., 2024b; Zhao and Dong, 2025; Heredia-Zavoni and Montes-Iturrizaga, 2019).

* Corresponding author.
E-mail address: p.maresnasarre@tudelft.nl (P. Mares-Nasarre).

https://doi.org/10.1016/j.oceaneng.2026.125487
Received 23 February 2026; Received in revised form 24 March 2026; Accepted 6 April 2026
Available online 17 April 2026

The interaction between the loading and the structure can be modeled using either deterministic or probabilistic methods. Traditionally in engineering, deterministic methods, from empirical equations to numerical models, are dominant in literature. Empirical equations are widely used to assess damage on rubble mound breakwaters and groynes (e.g. Mares-Nasarre et al., 2022; Vidal et al., 2006; Seemann et al., 2023) which are derived from scale laboratory experiments or field campaigns, being thus limited to the ranges of the variables analyzed by the authors. Numerical methods provide reasonable results for specific cases of study but at a high computational cost (e.g. Molines et al., 2020; Valela et al., 2021). Since these models are highly non-linear, high resolution on both the numerical mesh and the input data is required, hindering the use of these numerical models in practical design applications. In recent years, some authors have pointed out that the interaction between loading and structure might present uncertainties and, thus, be of a stochastic nature (Romano et al., 2015). This has led to the proposal of new methods with probabilistic structure responses (Mares-Nasarre et al., 2024c) to incorporate these uncertainties in their design and assessment.

Regarding the modeling of deterioration, it is common practice to assume that it is a Markov process, according to Barlow and Proschan (1965). This is, it is assumed that given $X(t)$, the values of $X(\tau)$ where $\tau > t$ are independent from the values of $X(\upsilon)$ where $\upsilon < t$. The most popular Markov processes to model stochastic deterioration are continuous-time Markov processes with independent increments such as the compound Poisson process (e.g. Zhang et al., 2017, 2016), the Gamma process (e.g. Van Noortwijk and Frangopol, 2004; Mercier et al., 2012) and the Gaussian process, also called Brownian motion with drift or Wiener process (e.g. Zhang et al., 2016; Luo et al., 2024). If the damage on a structure is modeled using a Gaussian process, it might get reduced in time, which is an unrealistic assumption most of the times. For instance, a dike whose height is modeled using a Gaussian process could increase, which is not realistic (van Noortwijk, 2009). Differently, Gamma and compound Poisson processes are jump processes, i.e. the increments are independent and non-negative. According to Singpurwalla and Wilson (1998), the main difference between them is that Compound Poisson processes have a finite number of jumps in finite time intervals, while Gamma processes have an infinite number of jumps in finite time intervals. Gamma processes are then suitable to model monotonic damage that accumulates gradually over time in small increments (van Noortwijk, 2009) such as erosive processes or fatigue. Riverine and coastal structures are usually constructed from loose material such as rocks or concrete armor units, so their deterioration is gradual. Consequently, Gamma processes seem a reasonable option to model their deterioration.

Gamma processes are usually quantified from observations, i.e. using several time series of the deterioration of the studied element retrieved in the same conditions (e.g. Okafor et al., 2023; Pan and Balakrishnan, 2011). Therefore, if those loading conditions change, it might be needed to quantify again the Gamma process performing a new measurement campaign or elicitation if quantified using expert opinions (Nicolai et al., 2007). This hinders the application of Gamma processes to assess the impact of changes in the loading conditions (e.g.: climate change or changes in ship traffic) in the survivability of the structure and, thus, adapt accordingly the maintenance strategy depending on the loading scenario.

In this study, a methodology to assess the survivability of structures under different loading scenarios is proposed. A procedure to generate synthetic timeseries of deterioration is defined using a combination of a Poisson distribution, a Bernoulli process and multivariate joint distributions. These synthetic time series of deterioration can be generated for different loading scenarios to explore the survivability of the structure in changing conditions without the need of new measurement campaigns. They are generated by conditionalizing the multivariate distribution of the loadings which is given by the vine-copula. A Gamma process is later quantified using the generated synthetic timeseries. The use of the proposed methodology is illustrated using the example of the deterioration of a groyne under the ship-wave attack. The paper is presented in six main sections. In Section 2, the case study of a groyne under ship-wave attack is presented. In Section 3, the modeling outline is defined and the required methods are described, namely bivariate copulas, vine-copulas and Gamma process. In Section 4, the modeling outline is applied to the case study, showing an example of the conditional survivability of the structure. In Section 5, the limitations and assumptions of the proposed model are discussed. Finally, in Section 6, the main conclusions are summarized.

2. Case study

In this section, the case study is presented: a rock-armored groyne under ship-wave attach. Ship-wave refers to the wave pattern that is generated by a ship as it passes through water. These waves are a result of the displacement of water caused by the hull of the vessel. Vessels generate a short-period V-shaped wave system (Kelvin wake) which is readily observed; additionally, displacement vessels can generate long-period waves which can carry considerable amounts of energy causing erosion to embankments and damage to hydraulic structures, amongst others. Groynes are hydraulic structures built perpendicular or oblique to the riverbank into the channel to control embankment erosion, trap sediment, and improve flow conditions in the main channel. As prominent hydraulic structures in estuarine waterways, groynes are prone to damaged by long-period ship waves. Fig. 1 shows a picture of the studied groyne, as well as its cross section.

First, an overview of the field campaign performed by Melling et al. (2021) is given with the focus on the data used in this research. After that, the processing of the armor scans following Mares-Nasarre et al. (2024a) to obtain the damage quantification is explained.

2.1. Field data

Melling et al. (2021) document in detail a monitored pilot study of innovative groyne designs in Juelssand, on the northern bank of the Lower Elbe Estuary along the main access channel to the Port of Hamburg. The groynes here are subject to high ship-wave loads which can manifest as damaging high-velocity turbulent overflows in the root and trunk area. Two previously damaged groynes were rebuilt using innovative designs aiming to improve the structure stability. Here, data from groyne G1, which was rebuilt with a recessed root, is further analyzed. The armor layer of G1 consisted of a rock grading CP90/250 with median particle size $D_{50} = 15$ cm, which according to CIRIA/CUR/CETMEF (2007) corresponds to the nominal diameter or equivalent cube size $D_{n50} \approx 12.6$ cm, where $D_{n50} = M/\rho$, being M the mass of the rock, and ρ the mass density of the rock; high-density iron-silicate rocks ($\rho = 3.7$ tonnes/m^3) were used. G1 presented a gentle lateral slope (V/H = 1/4 at the trunk, and 1/5 at the head) and a slight longitudinal inclination (1/77). The groyne crest was rounded and the recessed root area was constructed with a width of 25 m to allow the wave energy to bypass the structure and, thus, minimize the damage to the groyne. The recessed area was protected against scour using rocks and gabions.

After a trial phase, the official monitoring started in July 2015 and G1 was tracked until July 2016, when damage was too severe and the groyne was again rebuilt in the same recessed design but with a larger rock grading. This year of data used here includes laser scans of the groyne topography recorded at low tides and recordings of the ship generated waves. For the former, a stationary land-based 3D geodetic monitoring system was deployed to record the evolution of the erosion of the armor layer of the groyne. After the post-processing (see Melling et al., 2021, for more information), scans covering the whole length of the groyne were obtained with a resolution of 25 cm. However, it should be noted that the further the survey area from the laser location (i.e. towards the groyne tip), the higher the uncertainty of the scans.

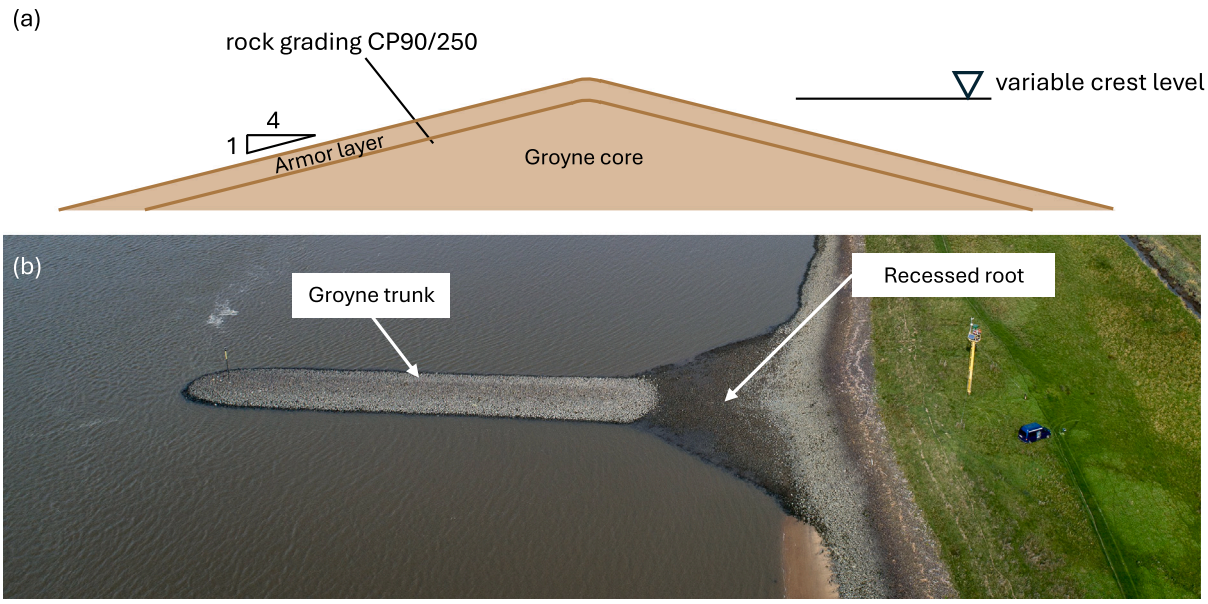

Fig. 1. Rock-armored groyne: (a) transverse trunk cross section, and (b) photo of the prototype. Photo provided by Federal Waterways Engineering and Research Institute, Germany.

Also, some laser scans needed to be disregarded due to insufficient data quality or obstructions such as seagulls sitting on the structure.

To measure ship wave heights, the water surface was measured at a frequency of 1 Hz at different locations around the structure. The raw signals of the sensors were processed to convert the pressure to water depth, filter the tidal contributions, filter the ship-induced components to obtain a clean signal of the long-period ship waves, and extract the wave events and determine the main variables to describe them. Example of such variables are the primary wave height, defined as the vertical distance between the minimum and maximum point of the primary wave, or the stern wave period, defined as the time between the drawdown and the stern wave.

Finally the identified ship-wave events were correlated to the data on vessel traffic from the Automatic Identification System (AIS) data. Thus, a final dataset relating the generated ship-induced waves and the ship variables of the generating vessel (e.g.: ship dimensions, draught, passing distance) was obtained. For further information about the uncertainties and treatment of AIS data, the reader is referred to Meyers et al. (2022) and Chen et al. (2025).

2.2. Damage analysis

The characterization of damage to the rock armor layer is performed using both quantitative and qualitative analysis. Here, the quantification of damage is performed using the dimensionless damage parameter, S_e, as defined by Broderick (1983).

$$S_e = \frac{A_e}{D_{n50}^2} \tag{1}$$

where A_e is the eroded area in a cross-section. To determine this area, a reference scan after the reconstruction of the groyne (here the one from 10th July) is compared to the subsequent scans and the eroded area between them is integrated. The following operations were conducted to improve the quantification of damage through that procedure: (1) linear interpolation between the observations to obtain the same grid in all the scans, (2) alignment of the cross-sections using as a reference point the highest point of the reference scan (no erosion), and (3) accounting only for the points where the difference with the reference scan was higher than 5 cm (see Fig. 2(b)).

This procedure was repeated with three cross-sections to characterize the biggest defect, which was located close to the recess, in alignment with reports in Melling et al. (2021). Once A_e was calculated for all the cross-sections, S_e was calculated using Eq. (1) and cumulative curves were obtained. In the case where $S_{e,i} > S_{e,i+1}$ for $i = 1, \ldots, N$, where N is the number of laser scans, $S_{e,i} = S_{e,i+1}$. Fig. 2(c) presents the obtained cumulative damage curves, while Fig. 2(a) shows the reference scan together with the location of the analyzed cross-sections.

Once the damage is quantified, the magnitude of the damage is translated into severity, as it relates to structure integrity, using qualitative damage levels. Losada et al. (1986) and Vidal et al. (1991) defined four qualitative levels of damage:

1. Initiation of Damage (IDa): the upper armor has lost some elements causing holes whose size is close to the armor unit;
2. Initiation of Iribarren's Damage (IIDa): a large area of the upper armor is eroded so the units from the bottom armor layer may be extracted.
3. Initiation of Destruction (IDe): the filter is exposed since at least one element from the bottom armor layer is extracted;
4. Destruction (De): elements from the filter layer are washed away.

Those qualitative levels are related to quantitative values of damage. Based on the recommendations for rubble mound breakwaters in shallow waters (Mares-Nasarre et al., 2021; Herrera et al., 2017), the following qualitative damage levels will be used: $S_e(IDa) = 0.5$, $S_e(IIDa) = 2$, $S_e(IDe) = 6$ and an additional extreme damage threshold case $S_e(-) = 10$.

2.3. Analysis of individual damage events

Each increase in the cumulative damage curves derived in Section 2.2 was correlated to one ship-wave event. Thus, the damage increment (ΔS_e) was associated with a concomitant ship passage and ship-induced wave as the largest event which happened between that scan and the previous one.

The curves obtained from the field are in terms of cumulative damage. It has been argued in the literature that for some typologies of hydraulic structures higher levels of pre-existing damage may lead to a larger increment of damage in the subsequent loading cycle, as the cross section might have lost part of its protection (Lira-Loarca et al.,

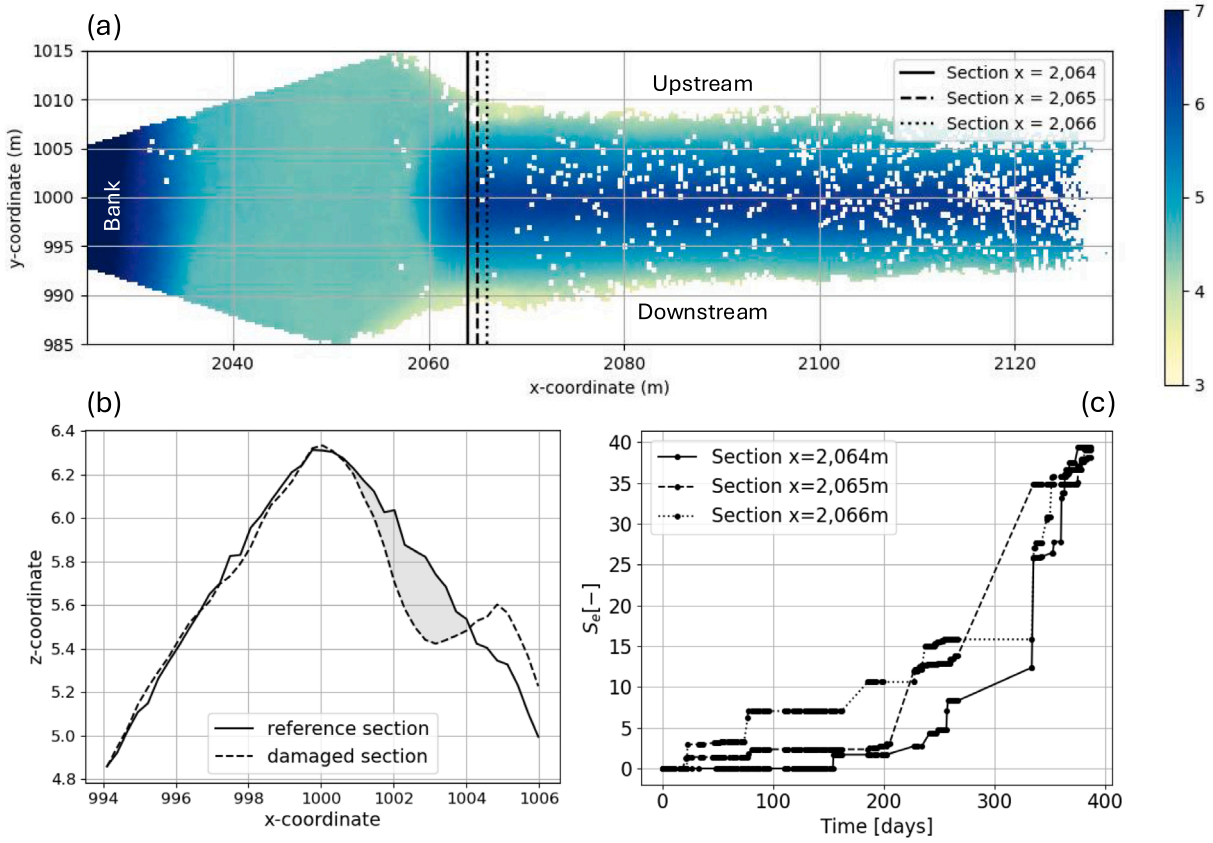

Fig. 2. Damage computation based on the field laser scans: (a) reference scan and location of the analyzed cross-sections with colors representing z-coordinate in meters, (b) example of eroded area computation, and (c) computed cumulative damage curves over time.

Table 1
Correlation analysis of the time series of damage.

Cross section	$R(S_{e,t}, \Delta S_{e,t+1})$	$p-value$ $(S_{e,t}, \Delta S_{e,t+1})$	$R(S_{e,t}, \Delta S_{e,t+2})$	$p-value$ $(S_{e,t}, \Delta S_{e,t+2})$
x = 2064 m	−0.29	<0.01	−0.29	<0.01
x = 2065 m	−0.06	0.33	−0.05	0.39
x = 2066 m	−0.07	0.28	−0.07	0.30

2020) and/or the defects might lead to more turbulent flow around it (Hoffmans, 2012). Thus, a key step to model them is to know if the pre-existing damage conditionalizes the increment of damage due to a next wave event (memory of the process). In order to determine that, the Spearman's correlation coefficient (Spearman, 1904; Glasser and Winter, 1961) was calculated between the damage at time step t and the increment of damage in the time step $t+1$. Spearman's correlation coefficient is defined as

$$R = \frac{Cov[Rank(X), Rank(Y)]}{\sigma_{Rank(X)}\sigma_{Rank(Y)}} \tag{2}$$

where $Cov[Rank(X), Rank(Y)]$ is the covariance of the ranked random variables, and $\sigma_{Rank(X)}$ and $\sigma_{Rank(Y)}$ are the standard deviations of the ranked random variables. Thus, R assesses the direction and strength of the association between two ranked random variables. $R \in [-1, 1]$, where $R = 1$ and -1 correspond to a perfect positive and negative monotonic dependence, respectively. Table 1 presents the results for the correlation analysis between $S_{e,t}$ and $\Delta S_{e,t+1}$, and $S_{e,t}$ and $\Delta S_{e,t+2}$.

As shown in Table 1, rank correlations in the range in $-0.29 \leq R \leq -0.05$ were obtained with most of $p-values > 0.05$, meaning that the observed correlations were mainly found not to be significant. Therefore, the increments of S_e, denoted as ΔS_e, were modeled independently in this study.

3. Modeling outline

The goal of this study is to propose a model capable of assessing the survivability of a structure accounting for possible changes in loading boundary conditions. The following methodology is proposed:

1. A Poisson distribution is used to model the number of loading events in the study location, here the number of passing ships.
2. A vine-copula (Czado, 2019) is used to model the joint distribution of the loading variables, here the primary wave height (H_p) and a set of explanatory variables. This model is used to generate the number of daily random samples given by the Poisson distribution to generate life cycles of H_p attacking the structure. Here, life cycles of 1 year are simulated, as this represents the timeframe from reconstruction to severe damage of the studied structure (see Section 2). Note that this model can be used to obtain the conditional distribution of a loading variable given that one of the other variables in the vine-copula are modified.
3. A bivariate copula together with a Bernoulli process is used to model the relationship between the main loading variable, H_p, and the increment of damage. The Bernoulli process is used to determine whether the passing ship generates damage and if so, a bivariate copula is used to model the joint distribution of the loading variable and the increment of damage. This step allows to translate the generated time series of loading events into cumulative damage curves along the life cycles.
4. A Gamma process is used to model the survivability of the structure, which is quantified using the randomly-generated damage curves.

The methodology is illustrated in Fig. 3. The following sections describe the different steps in further detail.

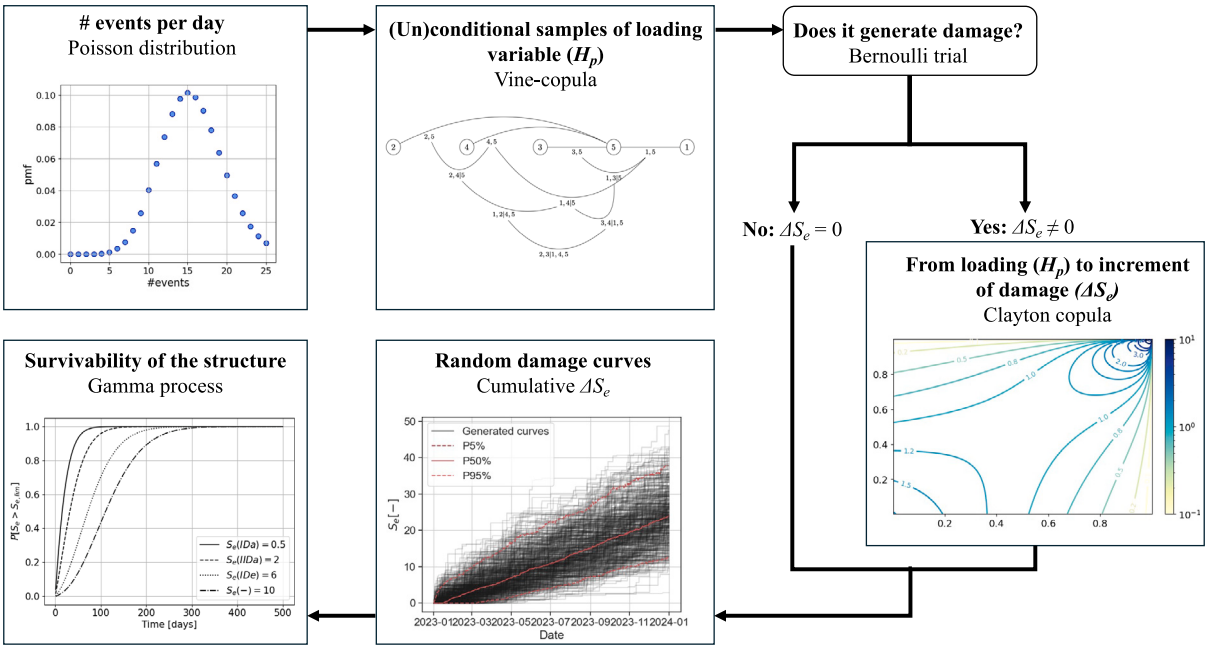

Fig. 3. Proposed methodology to assess the survivability of a infrastructure under conditional scenarios.

3.1. Poisson distribution

Poisson distribution is a discrete probability distribution with a constant intensity, λ, used to model the number of occurrences of an event in a time block (e.g. Tajiani et al., 2024; Amaya-Gómez et al., 2024). Here, the number of ship passages per day are modeled using a Poisson distribution, which is assumed equal regardless the day of the week. This assumption is validated using a Chi-square test comparing the distribution function of the number of ship passages between days. The null hypothesis of the Chi-square test is that the two samples come from the same distribution. Thus, $p-values$ below the significance level (here, 0.05) indicate a statistically significant difference. No significant differences were observed between any pair of days of the week.

3.2. Bivariate copulas

Bivariate copulas, or just copulas, are bivariate joint distributions with uniform marginal distributions in [0, 1]. According to Sklar (1959)'s theorem, any multivariate joint distribution of continuous variables can be described as a set of univariate marginal distributions and a copula that models the dependence between these variables. The definition of bivariate copula for the case is given by

$$H_{X,Y}(x,y) = C\{F_X(x), G_Y(y)\} \tag{3}$$

where $H_{X,Y}(x,y)$ for $(x,y) \in \mathbb{R}^2$ is a joint distribution with marginals $F_X(x)$ and $G_Y(y)$ in [0, 1] and a copula in the unit square $I^2 = ([0,1] \times [0,1])$, being Eq. (3) satisfied for all $(x,y) \in \mathbb{R}^2$.

Different families of copulas can be found in the literature (Czado, 2019). All the copula families implemented in the Python package Pyvinecopulib (Vatter and Nagler, 2022) are assessed here; the best fitting family in terms of Akaike Information Criterion, AIC, Akaike (1973) was chosen. AIC is given by

$$AIC = 2k - 2\hat{L} \tag{4}$$

where k is the number of parameters in the model and $\hat{L}$ is the log-likelihood. Thus, AIC penalizes a higher number of parameters.

The selected copula family is further validated using the Cramer-von-Mises statistic, S_{CvM} (Genest et al., 2009). S_{CvM} evaluates the distance between the fitted parametric copula and the empirical copula. Thus, the better the fit, the lower the S_{CvM}, being the perfect fit given by $S_{CvM} \to 0$. S_{CvM} is defined as

$$S_{CvM}(\mathbf{u}) = n \sum_{|n|} \{C_n(\mathbf{u}) - C_{\hat{\theta}_n}(\mathbf{u})\}, \mathbf{u} \in [0,1]^2 \tag{5}$$

where $C_n(\mathbf{u}) = \frac{1}{n}\sum_{i=1}^{n} \mathbf{1}(U_i \leq \mathbf{u})$ is the empirical copula and $C_{\hat{\theta}_n}(\mathbf{u})$ is the fitted parametric copula with parameter $\hat{\theta}_n$ estimated from the sample.

One distinctive feature between copula families is tail dependence which characterizes the correlations in the tails of the distributions of random variables. The *upper* tail dependence coefficient is defined as $\lambda_u = \lim_{t \to 1^-} P(X_2 > F_2^{-1}(t) | X_1 > F_1^{-1}(t))$ (Sibuya et al., 1960; Joe, 1997). The reader is referred to Nelsen (2006) for further information about copulas.

3.3. Vine-copulas

A vine-copula is composed of a series of nested trees which model the dependence in bivariate pieces via conditionalizing. Joe (1996) gave the first pair copula construction for a multivariate copula in terms of distribution functions, while Bedford and Cooke (2001) independently proposed constructions in terms of densities. Here, some basic definitions are provided. For further treatment, the reader is referred to Czado (2019).

A tree is a undirected acyclic graph $T = \{N, E\}$ labeled with nodes $N = \{1, 2, \ldots, d\}$ and edges E, being E a subset of pairs of N with no cycle.

A regular vine, V, on d elements is a sequence of trees $T_1, \ldots, T_{d-1}$ which fulfills the following conditions: (1) T_1 is a tree with node set $N_1 = \{1, \ldots, d\}$ and edge set E_1, (2) T_j is a tree with node set $N_j = E_{j-1}$ and edge set E_j for $j \geq 2$, and (3) for $j = 2, \ldots, d-1$ and $(a,c) \in E_j$, it must hold that $|a \cap c| = 1$. Condition (3), also called the proximity condition, ensures that if there is an edge e connecting a and c in tree T_j, $j \geq 2$, then a and c (being edges in T_{j-1}) must share a common node in T_{j-1}. Therefore, a regular vine on d elements is that in which two edges in tree j are joined by an edge in tree $j+1$ if these edges are sharing a common node in tree j.

For $e \in E_j$, $j \leq d-1$, the constraint set associated with e is the complete union U_e^* of e. This is, the subset of $N_1 = \{1, \ldots, d\}$ reachable from e by the membership relation. For $j = 1, \ldots, d-1$, $e \in E$ if $e = \{i, k\}$ then the conditioning set associated with e is $D_e = \{U_i^* \cap U_k^*\}$ and the

conditioned set associated with e is $\{C_{e,i}, C_{e,k}\} = \{U_i^* \setminus D_e, U_k^* \setminus D_e\}$. Note that the conditioning set is empty for $e \in E_1$ and that the order of an edge is the cardinality of its conditioning set. For $e \in E_j$, $j \leq d-1$, $e = \{i,k\}$, $U_e^* = U_i \cup U_k^*$. Therefore, nodes in T_1 reachable from a given edge via the membership relation are elements of the constraint set of that edge. When two edges in T_j are joined by an edge in T_{j+1}, the intersection of the respective constraint sets forms the *conditioning* set. The symmetric difference of the constraint sets is the *conditioned* set of this edge.

Bedford and Cooke (2001) show that a vine-copula can be uniquely connected to a d-dimensional distribution F, given as

$$F_{C_{e,i}C_{e,k}|D_e}\left(x_{C_{e,i}}, x_{C_{e,k}}|x_{D_e}\right) = C_e\left(F_{C_{e,i}|D_e}\left(x_{C_{e,i}}|x_{D_e}\right), F_{C_{e,k}|D_e}\left(x_{C_{e,k}}|x_{D_e}\right)\right) \quad (6)$$

where the one dimensional distributions of F are given by $F_m(x_m)$, $m = 1, \ldots, d$.

In short, in the first tree of a vine copula, each node represents one variable, and each arc represents the dependence between the two variables and is quantified using a bivariate copula. In the subsequent trees, the nodes are the bivariate copulas in the previous tree, and the arcs are quantified with conditional bivariate copulas that connect nodes with a common variable. Thus, the definition of a vine-copula involves defining both the regular vine (graph), and the fitted copulas that model the dependence between each (un)conditional pair.

3.4. Univariate marginal distributions

Each random variable is modeled here using a parametric distribution function in order to be able to infer values whose probabilities have not been observed in the dataset. A list of 13 parametric distribution functions is considered: (1) lognormal, (2) normal, (3) exponential, (4) Generalized Extreme Value, (5) Gumbel, (6) left-tailed Gumbel, (7) beta, (8) Rayleigh, (9) uniform, (10) gamma, (11) Generalized Pareto, (12) truncated normal, and (13) student t. AIC and visual inspection are used to select the parametric distribution functions to model each random variable. Results can be found in Appendix A.

3.5. Gamma process

A gamma process is a stochastic process with independent, non-negative increments which have a gamma distribution with an identical scale parameter. According to van Noortwijk (2009) and Abdel-Hameed (1975) was the first to propose the gamma process as a proper model for deterioration occurring random in time. The gamma process is suitable to model gradual damage monotonically accumulating over time in a sequence of tiny increments. van Noortwijk (2009) provides as an example of a gamma deterioration the settlement of the dike crest; dikes can only decrease in height due to crest-level decline.

The gamma process is mathematically defined as follows. X has a gamma distribution with shape parameter $v > 0$ and scale parameter $u > 0$ if its probability density function is given by

$$Ga(x|v,u) = \frac{u^v}{\Gamma(v)} x^{v-1} exp(-ux) I_{(0,\infty)}(x) \quad (7)$$

where $I_A(x) = 1$ for $x \in A$ and $I_A(x) = 0$ for $x \notin A$ and $\Gamma(a) = \int_{z=0}^{\infty} z^{a-1}e^{-z}dz$ is the gamma function for $a > 0$. Furthermore, let $v(t)$ be a non-decreasing, right-continuous, real-valued function for $t \geq 0$, with $v(0) \equiv 0$. The gamma process with shape function $v(t) > 0$ and scale parameter $u > 0$ is a continuous-time stochastic process $X(t), t \geq 0$ with the following properties:

1. $X(0) = 0$ with probability one;
2. $X(\tau) - X(t) \sim Ga(v(\tau) - v(t), u)$ for all $\tau > t \geq 0$;
3. $X(t)$ has independent increments

In our case, failure of a component is defined as the moment when the resistance, $R(t) = r_0 - s$, drops below the stress s, being r_0 the initial resistance. Assuming that r_0 and s are known, it is possible to define $y = r_0 - s$ and denote the time at which the failure occurs as T_y. The lifetime distribution is given by

$$P[T_y \leq t] = P[X(t) \geq y] = \int_{x=y}^{\infty} f_{X(t)}(x)dt = \frac{\Gamma(v(t), yu)}{\Gamma v(t)} \quad (8)$$

where $\Gamma(a,x) = \int_{z=x}^{\infty} z^{a-1}e^{-z}dz$ is the incomplete gamma function for $x \geq 0$ and $a > 0$.

In order to quantify the Gamma process, here the Methods of Moments is applied. The expected value and variance of the accumulated deterioration at time t assuming that it is proportional to a power law are given by

$$E(X(t)) = \frac{ct^b}{u}, \; Var(X(t)) = \frac{ct^b}{u^2} \quad (9)$$

where $v(t) = ct^b$ for $c > 0$ and $b > 0$. Ellingwood and Mori (1993) provides examples of expected deterioration according to a power law for concrete degradation due to corrosion ($b = 1$), sulphate attack ($b = 2$) or diffusion-controlled aging ($b = 0.5$). If the expected deterioration is linear in time, i.e., $b = 1$, the Gamma process is called stationary.

4. Building the model

Here, the results of the different modeling phases in the methodology in Section 3 are presented. First, a Poisson distribution is used to model the number of ship passages each day (see Section 3.1). The Poisson distribution is fitted using the property of the Poisson distribution where $E(X) = \lambda = 15.55$. A vine-copula (Czado, 2019) is used to model the joint distribution of ship passages and the generated primary wave heights, similar to Mares-Nasarre et al. (2024b). Afterwards, the relationship between the primary wave height and ΔS_e is modeled with a Bernoulli process together with a bivariate copula. This step allows to translate the generated primary wave heights into cumulative damage curves along the life cycles. Finally, a Gamma process is quantified using the generated curves.

In the following sections, the results related to the vine-copula used to model the dependence of ship-induced waves, the random damage curves and the Gamma process are presented.

4.1. Dependence model for ship-induced waves

In this section, first, the variables to include in the model are discussed based on the existing literature. These variables are depicted in Fig. 4. Afterwards, the quantification of the model is discussed and the proposed vine-copula is presented.

The first variable to include in the dependence model is the target variable directly related to the armor erosion of the structure: the primary wave height, H_p (m). Afterwards, the Spearman's rank correlation coefficient (Spearman, 1904) is calculated in pairs between H_p and each available variable in the field dataset. Rank correlation coefficient assesses the strength of monotonic dependence between two random variables and is used here to identify the best explanatory variables for H_p. P-values associated with those rank correlations are also computed to identify whether the computed correlations are significant. Based on the aforementioned analysis, five explanatory variables are identified and included in the model together with H_p. The six total variables included in the model are:

1. Primary wave height (H_p, m), defined as the vertical distance between the minimum and maximum point of the primary wave. H_p is a good proxy for the energy of the event (Muscalus et al., 2024) and is the most relevant variable for assessing the damage on groynes due to overflow (Melling et al., 2021; Memar et al., 2025).

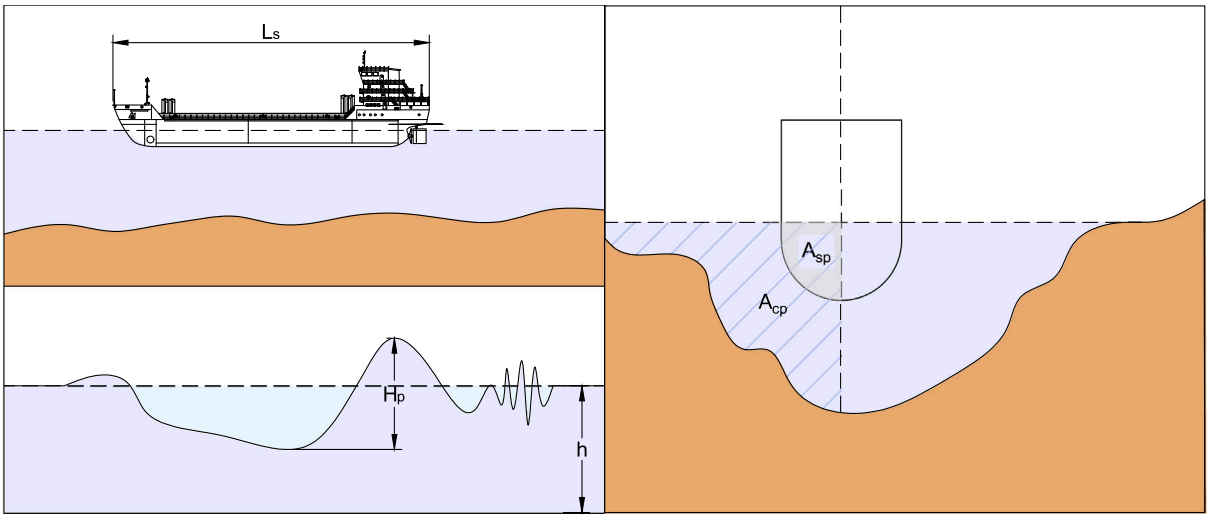

Fig. 4. Definition of the ship-wave variables discussed in this study.

2. Relative speed of the ship (V, m/s), defined as the velocity through water from AIS data calculated accounting for the flow velocity from a hydrodynamic model. V is widely accepted as a variable that governs the ship-induced loads (Schijf, 1949; Gelencser, 1977; Dand and White, 1978; Bhowmik et al., 1981; Hochstein, 1967; Maynord, 1996; Kriebel et al., 1996; CIRIA and CUR, 2007; Almstrom and Larsön, 2020; Memar et al., 2025). Moreover, not only the larger but also the faster ships have been found to produce larger primary waves (Bain et al., 2022; Muscalus et al., 2024). As a consequence, ship speed restrictions are common practice in waterways to limit the impact of ship-induced loads (Melling et al., 2019).
3. Ship length (L_s, m). L_s is included in most empirical equations for assessing the ship-induced waves (Gelencser, 1977; Bhowmik et al., 1981; Kriebel et al., 1996). Typically, larger ships are associated with larger primary ship waves (Almstrom and Larsön, 2020; Bain et al., 2022; Muscalus et al., 2024).
4. Ship width (W_s, m). Several studies discuss the influence of ship dimensions on the generated ship-induced waves, including variables related to the ship width such as the ship cross-section (Schijf, 1949; Gelencser, 1977; Dand and White, 1978; Bhowmik et al., 1981; Hochstein, 1967; Maynord, 1996; CIRIA and CUR, 2007). It should be also noted that ship length and ship width are more accessible and reliably accurate in AIS data than ship cross-section.
5. Partial blockage factor ($nT = A_{sp}/A_{cp}$ (-), where A_{sp} is the ship's immersed cross-section from the ship centerline and A_{cp} is the waterway's cross-section from the ship centerline). Melling et al. (2021) introduced this variable to account for the passing distance from the ship centerline to the point of interest, being later used in Memar et al. (2025). This variable accounts for the portion of water volume that is displaced by the passing ship. Therefore, it includes other variables such as the waterway water level or the ship draught. The commonly used blockage factor ($C_H = D_s \cdot W_s / A_{channel}$ (-), where D_s is the ship draught and $A_{channel}$ is the cross-sectional area of the waterway) is commonly considered in primary wave observational and experimental studies (Kriebel et al., 1996).

As described in Section 3.3, the definition of a vine-copula implies the definition of a regular vine (graph) and the bivariate copulas which quantify its edges. As shown in Morales-Nápoles (2010), the number of regular vines grows extremely quickly with the number of nodes. For five variables, 480 regular vines (graphs) are possible. Here, all possible regular vines are fitted using the atlas Chimera (Morales-Nápoles et al., 2023), and the best model in terms of AIC is selected, similar to previous studies (Mares-Nasarre et al., 2024b; 't Hart et al., 2024). Further information about the robustness of the selected vine-copula model is presented in Appendix C. All the bivariate copula families included in Vatter and Nagler (2022) are considered. The obtained dependence model to describe the joint probability of the selected variables is depicted in Fig. 5.

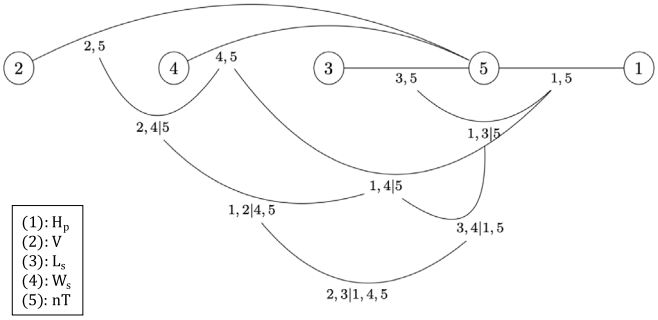

Fig. 5. Multivariate dependence model: regular vine.

Fig. 6 presents the scatter matrix with 10,000 samples and probability densities obtained using the aforementioned model.

4.2. From loading to cumulative damage curves

As exposed in Section 3, for each day, the number of ship-induced events is modeled using a Poisson distribution. For each event, a conditional or unconditional sample of H_p can be obtained from the dependence model in Section 4.1. Afterwards, the relationship between the environmental variables and the damage is modeled through a bivariate copula between H_p and ΔS_e and a Bernoulli process. The Bernoulli process determines whether the event generates damage, with probability of success $p = 0.003$. For those events which generate damage, a conditional sample of ΔS_e is obtained with the copula between H_p and ΔS_e. The best fitting copula for that pair of variables in terms of AIC is a Clayton copula rotated 180° with $\delta = 0.766$ (Kendall rank correlation coefficient, Kendall, 1938, $\tau = 0.28$). Clayton copula is part of the Archimedean family and is parameterized by $\delta > 0$ and given by

$$C_\delta(u, v) = (u^{-\delta} + u^{-\delta} - 1)^{-1/\delta} \tag{10}$$

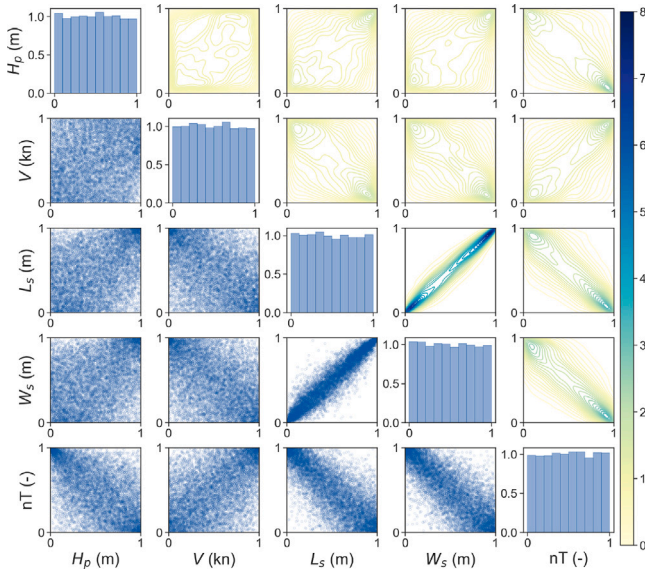

Fig. 6. Scatter matrix with 10,000 samples and probability densities.

where u and v are the random variables in (0, 1). Clayton copula presents lower tail dependence. This is, the low observations are more correlated to each other than the bigger ones. However, in this case, the Clayton copula is rotated 180°, which makes the tail dependence switch: the high values of H_p and ΔS_e are more correlated to each other than the low ones. As explained in Section 3.2, S_{CvM} is applied to better assess the goodness of fit of the selected model; $S_{CvM} = 0.56$ indicating a satisfactory performance of the rotated Clayton copula.

The sampled values of ΔS_e are transformed from copula to variable space through the inverse of its marginal distribution and accumulated in time, generating random damage curves along the life of the structure. Here, a life of 1 year is simulated 500 times, obtaining 500 random damage curves, as shown in Fig. 7(a).

4.3. Gamma process for survivability of groyne

In this study, a stationary Gamma process is assumed ($b = 1$ in Eq. (9)). Thus, c and u are computed using Eq. (9) together with the generated random damage curves in Fig. 7(a). For each time t, the mean and variance of S_e for the generated curves is computed and $c = 0.024$ and $u = 0.22$ are obtained. Further information about the fit is provided in Appendix D. Fig. 7(b) presents the results of the fitted gamma process for different damage levels. This gamma process can be used as input for maintenance scheduling and its optimization. For instance, if the maximum tolerable damage is $S_e(IDa) = 10$, after 200 days, there is a probability of 0.71 that damage level would have been reached.

4.4. Conditionalizing structure's survivability

Gamma process is a useful tool for modeling the survivability of the structure but it cannot be directly used to analyze the survivability of the structure under unseen loading scenarios. This is, if measures are taken to change the environmental conditions and, thus, limit the loading, the gamma process would need to be again quantified with new observations. Here, it is proposed to use the previously described methodology to simulate (conditional) cumulative damage curves under the desired scenario and quantify the survivability of the structure. Here, the example of a limitation of the relative velocity of the ship $V < 12\ kn$ is used. The outline of the methodology described in Section 3 is followed with one change: the random samples drawn from the vine-copula are now conditional samples on $V < 12\ kn$. Here, the conditionalization of the vine-copula is done through simulation. The subject of conditionalizing vine copulas is far from closed and an active research subject. For further information about conditional sampling of vine-copulas, the reader is referred to Czado (2019) and Hanebeck et al. (2025). Using the generated conditional damage curves, the Gamma process is quantified obtaining $c = 0.027$ and $u = 0.41$. Fig. 8(a) presents a comparison of the generated unconditional damage curves (same as Fig. 7(a)) and the generated damage curves when limiting the ship velocity. It can be observed how the conditional curves reach lower levels of damage.

Fig. 8(b) compares the unconditional (same as Fig. 7(b)) and conditional Gamma processes for different damage levels. The higher the assessed damage level, the largest difference between the probabilities along the design life of the structure. For instance, for a maximum tolerable damage of $S_e(IDa) = 2$, the probabilities of exceeding that damage level after 100 days are 0.966 and 0.922 for the unconditional and conditional process, respectively, while for a maximum tolerable damage of $S_e(IDa) = 10$, they are 0.466 and 0.175.

5. Discussion

In this research, a methodology to assess the survivability of riverine and coastal structures under different loading scenarios is defined. This methodology generates synthetic timeseries of deterioration using a combination of stochastic processes and multivariate joint distributions that are later used to quantify a Gamma process. In this process, increments of damage are generated and accumulated over time, leading to the synthetic timeseries of deterioration. These increments of damage at time t are assumed independent of the damage of the structure at time $t - 1$. This assumption was validated in the case study using the available observations through hypothesis testing (see Section 2.3). We hypothesize that the lack of observed dependence between the increment of damage at time t and the damage of the structure at time $t - 1$ might be caused by M_u/M_a, where M_u is M for the underlayer, and M_a is M for the armor. In conventional rubble mound breakwaters, $M_u/M_a = 1/15$ to $1/10$ (USACE, 1984) or $D_{n50,u}/D_{n50,a} = 0.4$ to 0.45 (CIRIA/CUR/CETMEF, 2007). Therefore, after the armor layer is eroded, loading starts attacking lighter rocks with a significantly lower resistance, accelerating the deterioration and making damage evolution dependent of the existing damage. According to Melling et al. (2021), for the groynes investigated, M_u is governed by the remnants of earlier groyne structures underlying the present construction; consequently, M_u may exceed the recommended range of $M_a/10$ to $M_a/15$. Consequently, after the armor layer is eroded, the underlayer elements might present a higher resistance than the one that would be provided by an underlayer with weights in the range $M_a/10$ to $M_a/15$, leading to a more linear damage evolution.

However, when comparing the observed and simulated damage curves for the case study, the simulated ones were more linear than the observed ones. A possible reason for that might be that there is some degree of dependence between the increment of damage at time t and the damage of the structure at time $t - 1$ that the hypothesis test was not able to detect.

In this case, the generated curves were on the conservative side: the 50th percentile of the predicted damage levels were approximately the same as those observed in the beginning and ending of the design life, while were superior around the middle of the design life. In case of facing a situation where the increment of damage at time t and the damage of the structure at time $t - 1$ are identified as not independent, the present methodology could be extended by accounting for the dependence between the existing damage at time $t - 1$ and the increment of damage at time t by means of dependence models such as bivariate copulas. Also, since the generated damage curves were approximately linear, here a stationary Gamma process was assumed ($b = 1$). However, if in a different application the shape of the damage

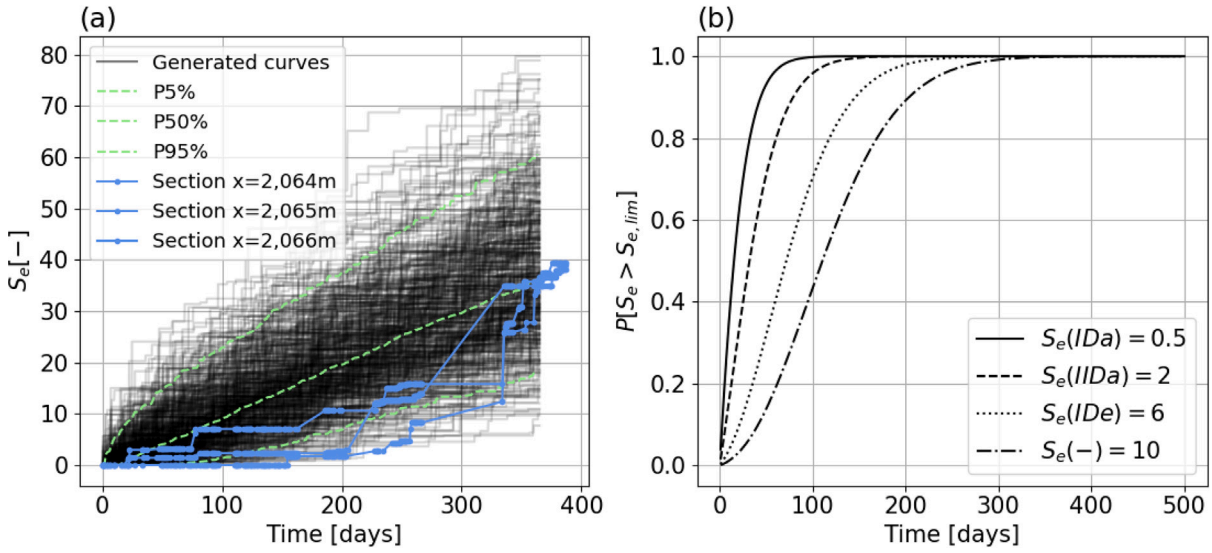

Fig. 7. Armor damage deterioration along the life of the structure: (a) observed and generated random damage curves, and (b) gamma process to describe the survivability of the structure.

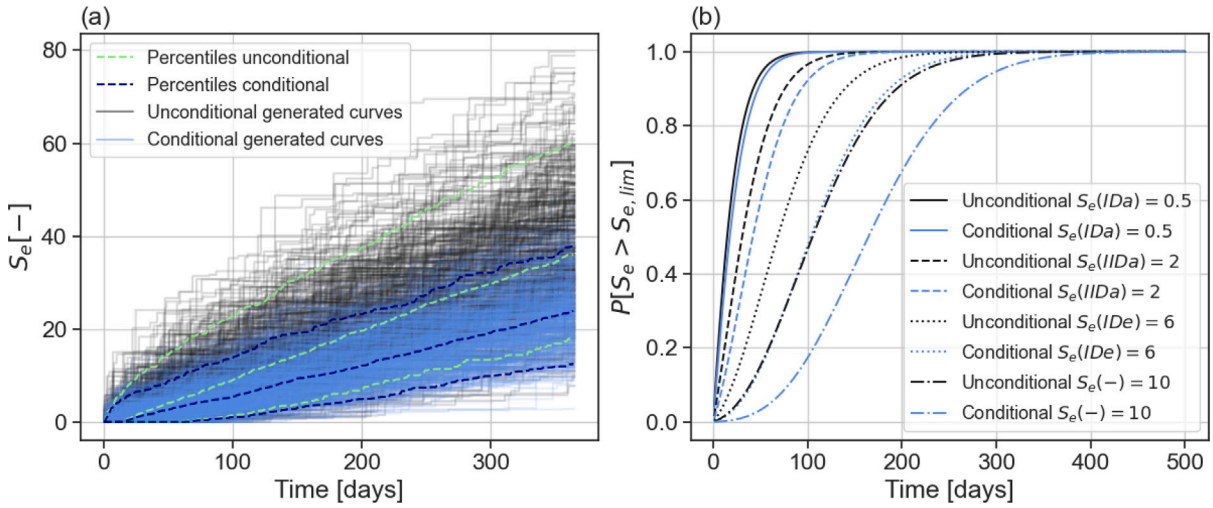

Fig. 8. Comparison of the armor damage deterioration along the life of the structure with (conditional) and without (unconditional) speed limitation: (a) generated random damage curves with 5%, 50% and 95% percentiles, and (b) gamma process to describe the survivability of the structure.

curves is not approximately linear, the parameter b could also be fitted to accommodate for different shapes of the damage curves.

The Gamma process used to assess the survivability of the structure is quantified first using unconditional damage curves and later using conditional curves under the scenario of a limitation of the relative velocity of the ship $V < 12\ kn$ (see Section 4.4). When comparing the quantification of both Gamma processes, the parameter c does not change significantly (unconditional $c = 0.024$, and conditional $c = 0.027$), while the parameter u doubles when conditionalizing (unconditional $u = 0.22$, and conditional $u = 0.41$). The parameter c is related to the frequency or rate at which the increments of deterioration occur, while u is related to the size of such increments. Therefore, it is expected that if the frequency of the loading changes, here modeled by a Poisson distribution (see Section 3.1), larger variations will occur in the parameter c. If the magnitude of the loading conditions (here H_p) or the resistance of the structure (here D_n) change, larger variations are expected to be observed in the parameter u, as seen in Section 4.4. However, the parameter c might also suffer variations under these conditions if the changes in the loading or resistance are such that the frequency of jumps in the deterioration significantly changes. For instance, if the structure is reinforced (e.g.: a relevant increase of the D_n) such that a much higher loading is required to make the deterioration grow, the frequency of increments in the deterioration will be reduced, and thus the parameter c.

Literature on long-term damage evolution of river groynes or rock-armored structures such as breakwaters is scarce. Methods in the literature (e.g. Lira-Loarca et al., 2020; Lucio et al., 2024) usually focus on the simulation of the hydraulic loadings, i.e. storm events, using statistical techniques to later quantify the damage evolution using empirical relationships. For instance, Lira-Loarca et al. (2020) and Lucio et al. (2024) used Gaussian copulas to model the multivariate distribution of the loadings. The assumption of Gaussian copulas, i.e. no tail dependence, is common practice in the Coastal Engineering field (e.g. Camus et al., 2019; Lucio et al., 2020) although tail dependence might be present and have a significant impact in design (Zhang et al., 2018; Kindermann et al., 2026). In this study, significant tail dependence is observed between the loading variables (see Fig. 6). Therefore, a vine-copula has been adopted to account for the asymmetries in the dependence structure as recommended in Mares-Nasarre et al. (2024b). To estimate the cumulative damage generated by the loadings, empirical equations such as those defined by Melby and Kobayashi (1999)

or Van der Meer (1988) are usually applied (Lira-Loarca et al., 2020; Lucio et al., 2024). Here, the translation of the loading into increments of damage is not done through a deterministic equation but using a bivariate copula. This is, the increments of damage directly depend on a single loading variable, H_p, whose relationship is modeled through a probabilistic model. This approach aims to account for the uncertainties in the ship-wave and structure interaction which in rubble mound structures may be derived from variations in the porosity, placement of the elements, geometry, and rock grading, between others (Mares-Nasarre, 2025).

The distribution of H_p is conditionalized given the observations of other random variables related to the generation of the ship-wave event through the vine-copula. Therefore, the synthetic timeseries can be generated under different loading scenarios by conditionalizing the multivariate joint distribution that describes the uncertainty of the loading variables. In the case study used here, the deterioration of a riverine groyne, H_p is considered the main loading variable according to the literature (Melling et al., 2021; Memar et al., 2025) and no other random variables are deemed relevant to directly model the increments of damage. However, if needed, the proposed framework could be extended to connect more than one loading variable with the increments of damage by means of a GCBN or another vine-copula. Moreover, this framework assumes that the response of the structure to the loading is always modeled by the same bivariate copula regardless of the changes in the loadings. This is, the proposed framework cannot take into account the influence of changes in the structure geometry (e.g.: slope or crest width), the properties of the elements that compose the armor layer (e.g.: D_{n50} or ρ) or unseen hydrodynamic behaviors of the armor layer. This limitation could be tackled if further data is available or through expert elicitation (Rongen et al., 2024; Ramousse et al., 2024).

Moreover, the present methodology considers the deterioration of the structure as the deterioration of a single defect driving a single failure mode. Therefore, it could be extended by considering the evolution of several defects, independent or dependent on each other (Barui et al., 2024; Dai et al., 2022), and competing failure modes (Haladuick and Dann, 2017; Zhang et al., 2016). For instance, a non-homogeneous Poisson process could be employed to model the generation of new defects (Zhang and Zhou, 2014; Yazdi et al., 2022), each of them growing independently following a Gamma process. Should it be desired to incorporate dependence among the growth of defects, a shared frailty term following a generalized gamma distribution may be employed (Barui et al., 2024).

The proposed methodology can be applied to other types of structures with a gradual deterioration. For instance, a direct extension of this study would be the deterioration of a mound breakwater under sea wave attack (Mares-Nasarre et al., 2022) or the erosion of river banks under ship-wave attack (Muscalus and Haas, 2022). Further applications within the Civil Engineering field could be the deterioration of pavement under traffic loading (Adegbola and Yuan, 2019) or the corrosion of steel due to environmental conditions such as moisture, temperature or Chloride concentration (Cai et al., 2020). In order to apply the proposed framework to other cases of study, it would be necessary to requantify both the multivariate distribution (both vine-copula and marginal distributions) and the Gamma process. To obtain data about loadings, existing datasets can be used if available (e.g. wave or water level historical records), or specific field campaigns can be performed. Data on the relationship between loading and degree of deterioration can be also gathered through field campaigns or physical model tests. Another option when quantify those models is elicitation using expert opinions applied to either the multivariate distributions (e.g. Rongen et al., 2024; Ramousse et al., 2024) or directly to the Gamma process (Nicolai et al., 2007).

6. Conclusions

In this paper, a methodology to assess the survivability of riverine and coastal structures under different loading scenarios is proposed. The methodology includes the coupling of multivariate joint distributions and stochastic processes to generate synthetic timeseries of deterioration used to quantify a Gamma process. A vine-copula is developed to model the joint distribution of the loadings in order to account for their asymmetries in the dependence structure. A bivariate copula is applied to transform the loadings into increments of damage, accounting for the uncertainties in ship-wave and structure interaction. By conditionalizing the joint distribution of the loading variables, it is possible to generate conditional synthetic damage curves and, thus, quantify a Gamma process conditional on the given loading conditions. This framework allows investigating what-if scenarios including changes in the loadings such as climate change, evolution of traffic or changes in the shipping fleet to better plan maintenance strategies for structures with gradual deterioration.

CRediT authorship contribution statement

Patricia Mares-Nasarre: Writing – original draft, Visualization, Methodology, Formal analysis, Data curation, Conceptualization. **Gregor Melling:** Writing – review & editing, Resources, Data curation. **Oswaldo Morales-Nápoles:** Writing – review & editing, Methodology, Funding acquisition, Conceptualization.

Declaration of competing interest

The authors declare that they have no known competing financial interests or personal relationships that could have appeared to influence the work reported in this paper.

Acknowledgments

The authors want to acknowledge the economic support of the project ProbBem, funded by the Federal Waterways Engineering and Research Institute (BAW, Germany).

Appendix A. Summary of univariate distribution functions

Here, a summary of the univariate distribution functions fitted to each studied random variable is presented in Table A.2.

Fig. A.9 shows the fit of the Generalized Pareto distribution (GPD) (cumulative distribution function in Eq. (A.1)) with parameters given in Table A.2 to the observations of H_p.

$$F_X(x) = \begin{cases} 1 - \left(1 + \frac{\xi_{GPD}(x-\mu_{GPD})}{\sigma_{GPD}}\right)^{-1/\xi_{GPD}} & \text{for } \xi_{GPD} \neq 0 \\ 1 - exp\left(-\frac{x-\mu_{GPD}}{\sigma_{GPD}}\right) & \text{for } \xi_{GPD} = 0 \end{cases} \tag{A.1}$$

where $x \geq \mu_{GPD}$ if $\xi_{GPD} \geq 0$, and $\mu_{GPD} \leq x \leq -\frac{\sigma_{GPD}}{\xi_{GPD}}$ if $\xi_{GPD} < 0$.

Fig. A.10 shows the fit of the Normal distribution (cumulative distribution function in Eq. (A.2)) with parameters given in Table A.2 to the observations of V.

$$F_X(x) = \frac{1}{2}\left(1 + \text{erf}\left(\frac{x-\mu}{\sigma\sqrt{2}}\right)\right) \tag{A.2}$$

where erf denotes the error function given by $\text{erf}(x) = \frac{2}{\sqrt{\pi}}\int_0^x e^{-t^2}dt$, and μ and σ are the mean and standard deviation of the random variable X.

Table A.2
Summary of univariate marginal distribution functions.

Variable	Parametric distribution	Parameters
Primary wave height, H_p (m)	Generalized Pareto	$\mu_{GPD} = 0$, $\sigma_{GPD} = 0.39$ and $\xi_{GPD} = -0.15$
Relative velocity of the ship, V (kn)	Normal	$\mu = 13.77$ and $\sigma = 2.03$
Ship length, L_s (m)	Uniform	$a = 101$ and $b = 299$
Ship width, W_s (m)	Rayleigh	$\mu_R = 13.77$ and $\sigma_R = 15.27$
Partial blockage factor, nT (–)	Gamma	$\alpha = 4.24$ and $\beta = 0.15$
Increment of damage, ΔS_e (–)	Exponential	$\lambda = 2.20$

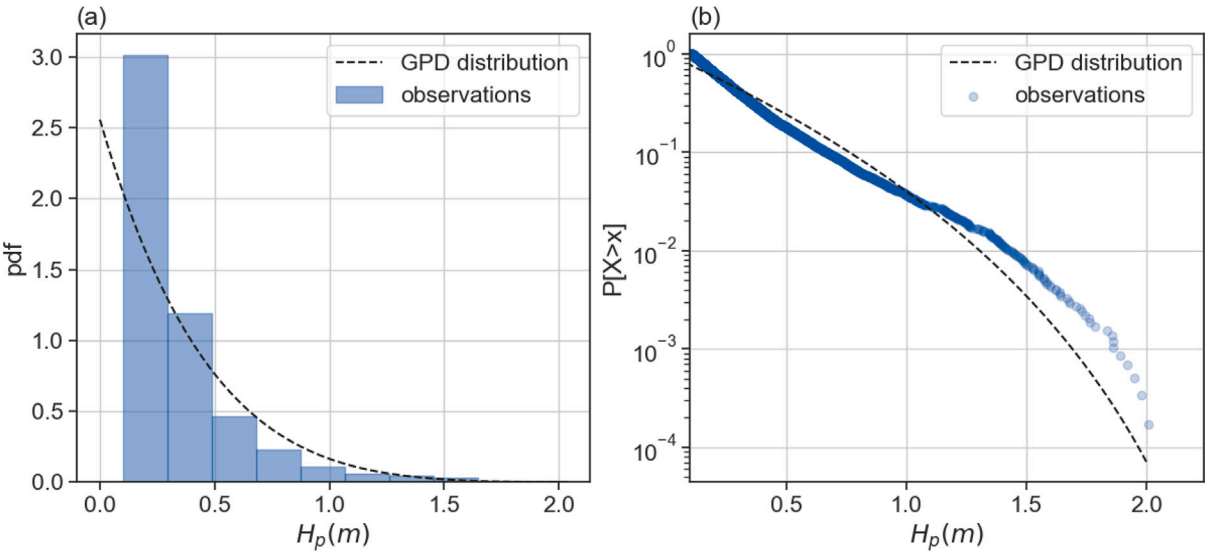

Fig. A.9. Empirical and fitted distribution function of H_p: (a) probability density function, and (b) cumulative distribution function.

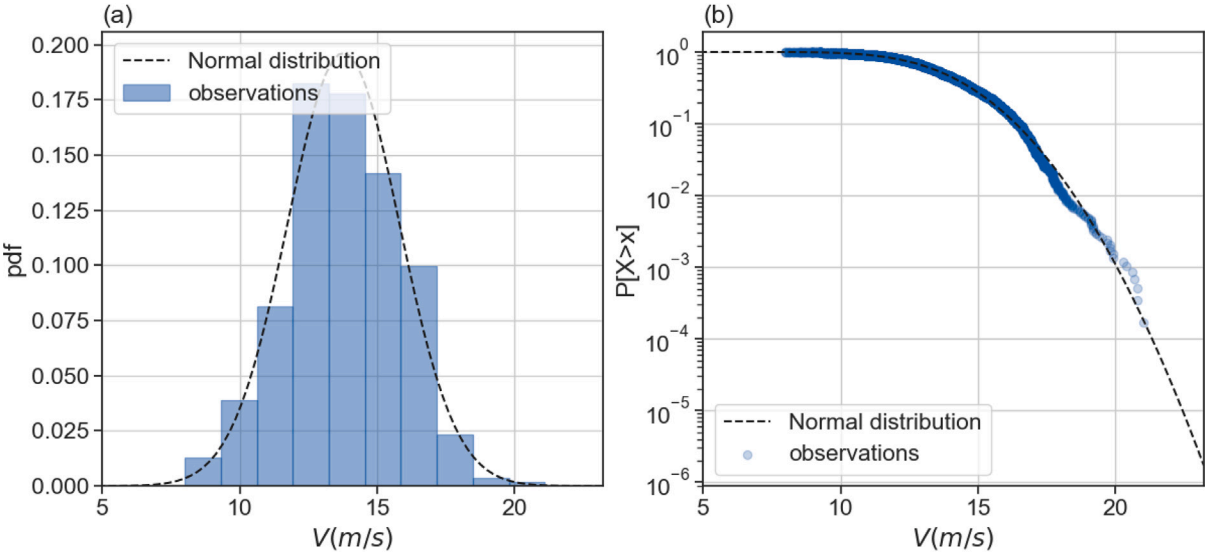

Fig. A.10. Empirical and fitted distribution function of V: (a) probability density function, and (b) cumulative distribution function.

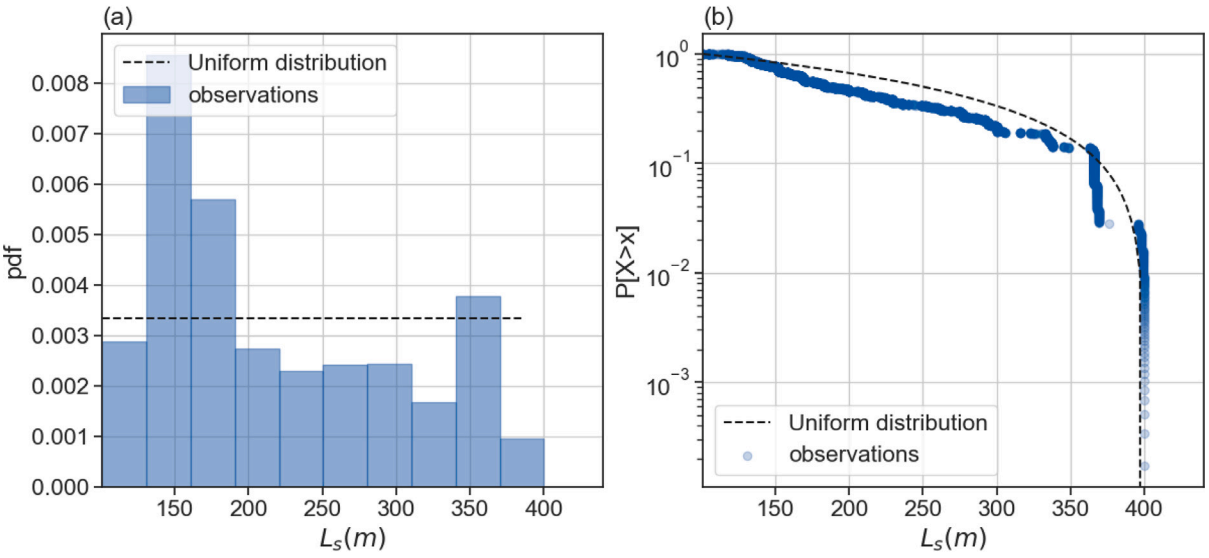

Fig. A.11. Empirical and fitted distribution function of L_s: (a) probability density function, and (b) cumulative distribution function.

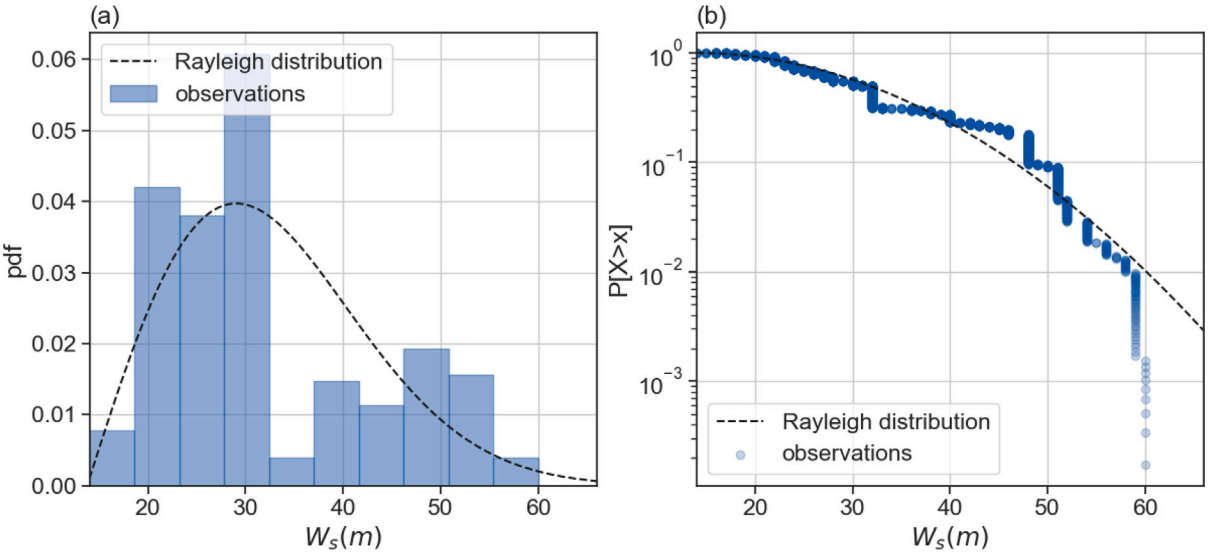

Fig. A.12. Empirical and fitted distribution function of W_s: (a) probability density function, and (b) cumulative distribution function.

Fig. A.11 shows the fit of the Uniform distribution (cumulative distribution function in Eq. (A.3)) with parameters given in Table A.2 to the observations of L_s.

$$F_X(x) = \begin{cases} 0 & \text{for } x < a \\ \frac{x-a}{b-a} & \text{for } a \le x \le b \\ 1 & \text{for } x > b \end{cases} \tag{A.3}$$

where a and b are the parameters of the distribution.

Fig. A.12 shows the fit of the Rayleigh distribution (cumulative distribution function in Eq. (A.4)) with parameters given in Table A.2 to the observations of W_s.

$$F_X(x) = 1 - e^{-(x-\mu_R)^2/2\sigma_R^2} \tag{A.4}$$

where μ_R and σ_R are the parameters of the distribution.

Fig. A.13 shows the fit of the Gamma distribution (cumulative distribution function in Eq. (A.5)) with parameters given in Table A.2 to the observations of nT.

$$F_X(x) = \frac{1}{\Gamma(\alpha)}\gamma(\alpha\beta x) \tag{A.5}$$

where α and β are the shape and rate parameters of the distribution, $\Gamma(\alpha)$ is the gamma function, and $\gamma(\alpha\beta x)$ is the incomplete gamma function.

Fig. A.14 shows the fit of the Exponential distribution (cumulative distribution function in Eq. (A.6)) with parameters given in Table A.2 to the observations of ΔS_e.

$$F_X(x) = \begin{cases} 0 & \text{for } x < 0 \\ 1 - e^{-\lambda x} & \text{for } x \ge 0 \end{cases} \tag{A.6}$$

where λ is the parameter of the distribution.

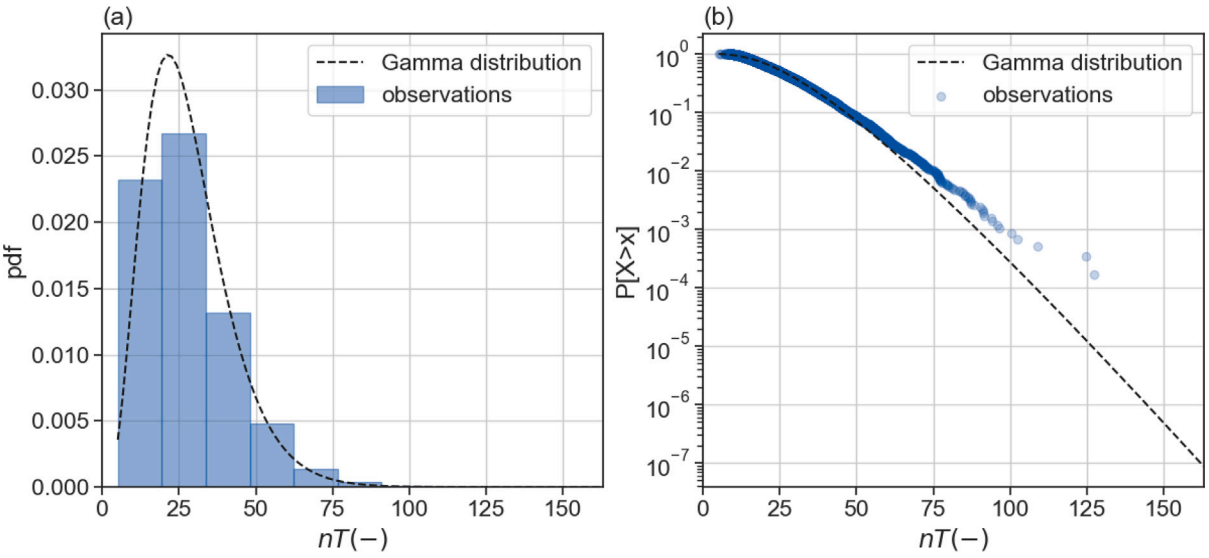

Fig. A.13. Empirical and fitted distribution function of nT: (a) probability density function, and (b) cumulative distribution function.

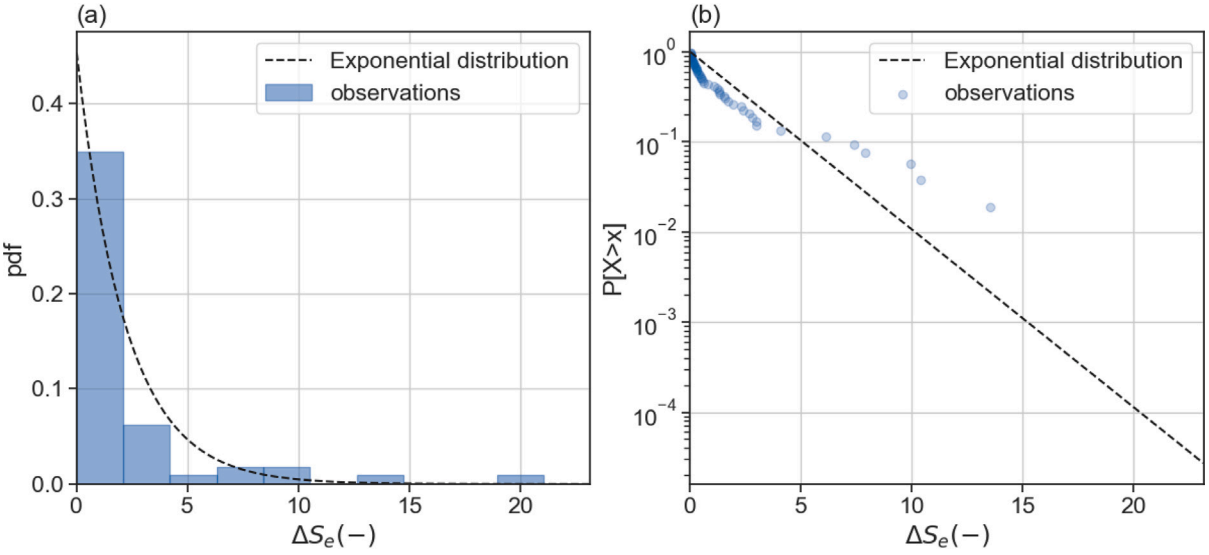

Fig. A.14. Empirical and fitted distribution function of S_e: (a) probability density function, and (b) cumulative distribution function.

Appendix B. Decomposition of the vine-copula model

The bivariate copulas used to quantify the arcs in the regular vine are the following.

Tree 1

2,5 - BB8, parameters = [3.38758, 0.717766]
4,5 - BB8 270°, parameters = [8, 0.646257]
1,5 - Gumbel 270°, parameters = 1.62136
5,3 - BB8 90°, parameters = [6.86583, 0.692365]

Tree 2

2,4 | 5 - BB8 270°, parameters = [1.4743, 0.735557]
4,1 | 5 - Frank, parameters = −1.15236
1,3 | 5 - Frank, parameters = −1.01969

Tree 3

2,1 | 4,5 - BB8, parameters = [4.58099, 0.720276]
4,3 | 1,5 - Student, parameters = [0.857886, 5.77237]

Tree 4

2,3 | 1,4,5 - BB8 180°, parameters = [1.12374, 0.975673]

Fig. B.15 shows the decomposition of the proposed regular vine-copula in dependence trees.

Appendix C. Vine-copula model fitting

In this section, further information about the fitting and selection of the vine-copula model is presented.

Fig. C.16 displays the distribution of AIC of the 480 possible regular vines. The model with the lowest AIC was chosen with AIC_{model} = −26064. In Fig. C.16, it can be seen that approximately 20% of the possible regular vines presented a value of AIC that differed from AIC_{model} less than a 4%.

An additional analysis is also performed to assess the robustness of the fit. 500 samples of length equal to the length of the observations, 5862 observations, are randomly generated from the selected model in Fig. 5. For each random sample, all possible regular vines are fitted using the atlas Chimera (Morales-Nápoles et al., 2023), and the best model in terms of AIC is selected. In 99.6% of the simulations, the same regular vine is selected as the best regular vine.

In addition, for each random sample, the minimum AIC is recorded and the obtained AIC from the Brute Force fitting, AIC_{model} = −26064, is put into the context of their distribution, as shown in Fig. C.17.

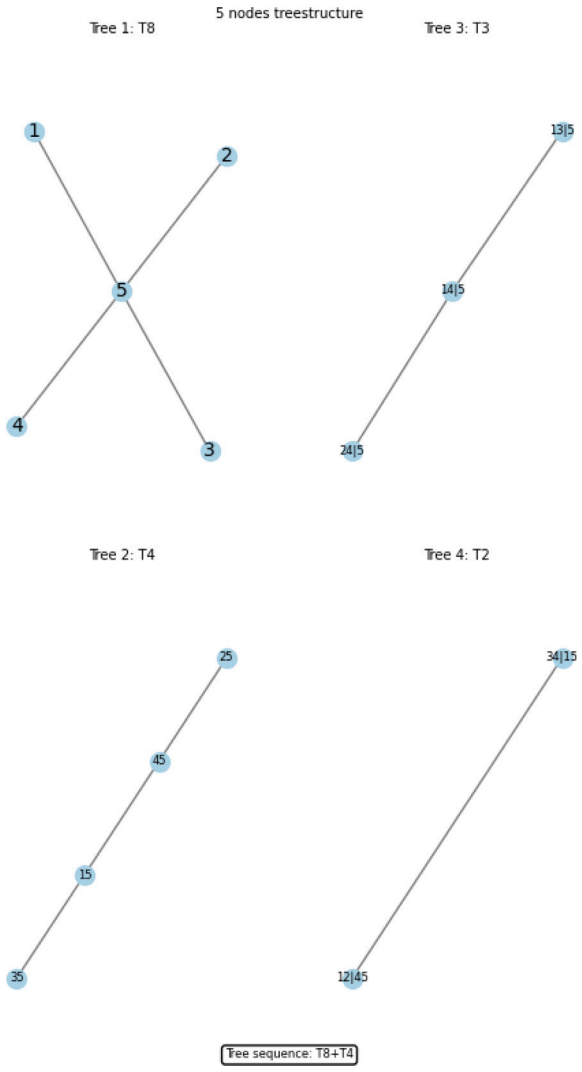

Fig. B.15. Vine-copula fitted using Brute Force.

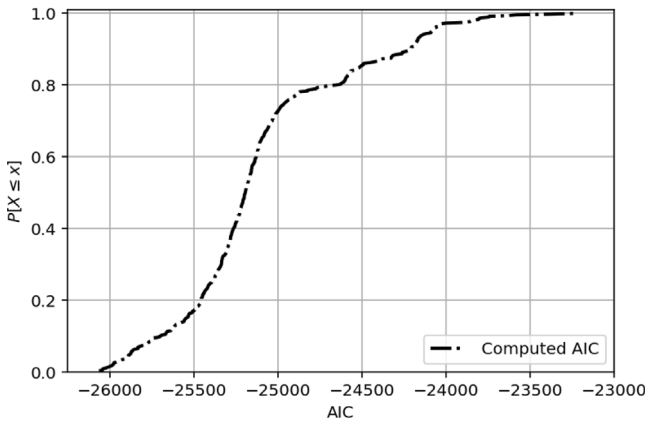

Fig. C.16. Distribution of AIC of the 480 fitted vine-copulas.

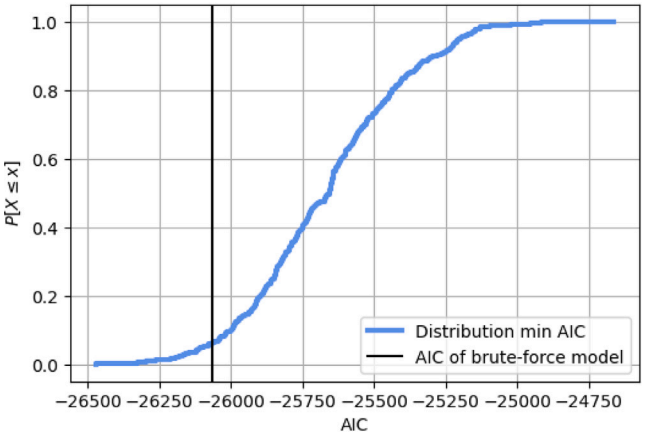

Fig. C.17. Distribution of the minimum AIC of the 500 simulations and AIC of the selected Brute Force model.

Appendix D. Gamma process fitting

Here, the fitting by moments of the Gamma process is assessed. Fig. D.18 presents the expectation and variance computed from the generated unconditional damage curves, and those fitted with $c = 0.024$ and $u = 0.22$. As it can be observed in Fig. D.18, the fit is almost perfect with coefficients of determination $R^2 > 0.99$.

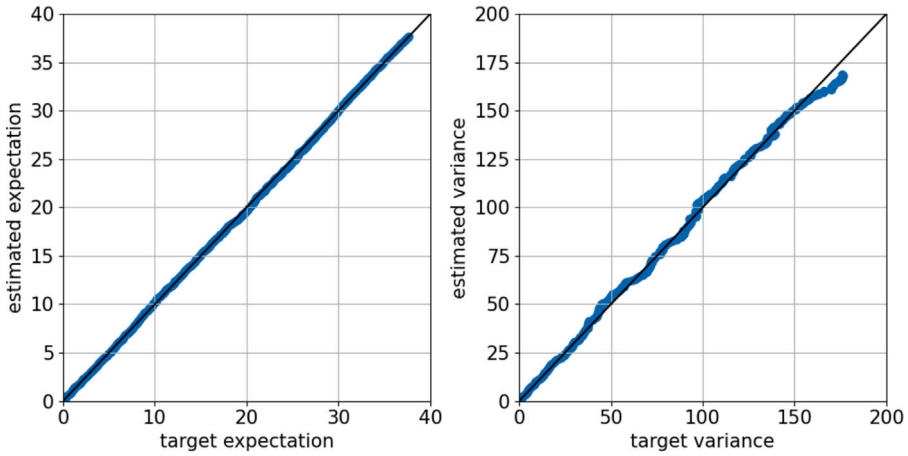

Fig. D.18. Comparison between (left) the expectation, and (right) variance, for each time t computed from the generated unconditional damage curves and those obtained with the fitting of the Gamma process.

References

Abdel-Hameed, M., 1975. A gamma wear process. IEEE Trans. Reliab. 24 (2), 152–153.

Adegbola, A., Yuan, X.-X., 2019. A multivariate gamma process for dependent degradation modelling and life prediction. In: 13th International Conference on Applications of Statistics and Probability in Civil Engineering. ICASP 2019.

Akaike, H., 1973. Information Theory and an Extension of the Maxmum Likelihood Principale. Akademia Kiado, pp. 267–281.

Almstrom, B., Larsön, M., 2020. Measurements and analysis of primary ship waves in the Stockholm archipelago, Sweden. J. Mar. Sci. Eng. 8, 743.

Amaya-Gómez, R., Sánchez-Silva, M., Muñoz, F., Schoefs, F., Bastidas-Arteaga, E., 2024. Spatial characterization and simulation of new defects in corroded pipeline based on in-line inspections. Reliab. Eng. Syst. Saf. 241, 109697.

ASCE, 2021. ASCE Report Card. Technical Report n.

Bain, R.L., Lopes, J.M., Styles, R., et al., 2022. Ship-Induced Waves at Tybee Island. Georgia.

Barlow, R.E., Proschan, F., 1965. Mathematical Theory of Reliability. Wiley, New York.

Barui, S., Mitra, D., Balakrishnan, N., 2024. Flexible modelling of a bivariate degradation process with a shared frailty and an application to fatigue crack data. Reliab. Eng. Syst. Saf. 242, 109722.

Bedford, T., Cooke, R.M., 2001. Probability density decomposition for conditionally dependent random variables modeled by vines. Ann. Math. Artif. Intell. 32, 245–268.

Bhowmik, N.G., Demissie, M., Osakada, S., 1981. Waves and Drawdown Generated by River Traffic on the Illinois and Mississipi Rivers. Technical Report n.

Broderick, L.L., 1983. Riprap stability. a progress report.. In: Proc. Specialty Conference on Design, Construction, Maintenane and Performance of Coastal Structures, ASCE, Arlington, VA. pp. 320–330.

Cai, Y., Xu, Y., Zhao, Y., Ma, X., 2020. Atmospheric corrosion prediction: a review. Corros. Rev. 38 (4), 299–321.

Camus, P., Tomás, A., Díaz-Hernández, G., Rodríguez, B., Izaguirre, C., Losada, I., 2019. Probabilistic assessment of port operation downtimes under climate change. Coast. Eng. 147, 12–24.

Chen, Y., Chen, Y., Cui, Y., Cai, X., Yin, C., Cheng, Y., 2025. Optimizing vessel trajectories: Advanced denoising and interpolation techniques for AIS data. Ocean Eng. 327, 120988.

CIRIA, CUR, C., 2007. The Rock Manual: The Use of Rock in Hydraulic Engineering. CIRIA publication, CIRIA.

CIRIA/CUR/CETMEF, 2007. The rock manual: The use of rock in hydraulic engineering.

Czado, C., 2019. Analyzing Dependent Data with Vine Copulas. Lecture Notes in Statistics, vol. 222, Springer.

Dai, X., Qu, S., Sui, H., Wu, P., 2022. Reliability modelling of wheel wear deterioration using conditional bivariate gamma processes and Bayesian hierarchical models. Reliab. Eng. Syst. Saf. 226, 108710.

Dand, I.W., White, W.R., 1978. Design of navigation canals. In: Proceedings of the 2nd Symposium Aspects of Navigability of Constraint Waterways, Including Harbor Entrances. Delft, Th Netherlands. pp. 1–9.

Ellingwood, B.R., Mori, Y., 1993. Probabilistic methods for condition assessment and life prediction of concrete structures in nuclear power plants. Nucl. Eng. Des. 142 (2), 155–166.

Gelencser, G., 1977. Drawdown surge and slope protection, experimental results. In: Proceedings of 24th International Navigation Congress, Leningrad, Soviet Union.

Genest, C., Rémillard, B., Beaudoin, D., 2009. Goodness-of-fit tests for copulas: A review and a power study. Insurance Math. Econom. 44 (2), 199–213.

Glasser, G.J., Winter, R.F., 1961. Critical values of the coefficient of rank correlation for testing the hypothesis of independence. Biometrika 48 (3/4), 444–448.

Haladuick, S., Dann, M.R., 2017. Risk-based maintenance planning for deteriorating pressure vessels with multiple defects. J. Press. Vessel. Technol. 139 (4), 041602.

Hanebeck, A., Şahin, Ö., Havlíčková, P., Czado, C., 2025. Sampling from conditional distributions of simplified vines. Stat. Comput. 35, 128.

Haralambides, H., 2017. Globalization, public sector reform, and the role of ports in international supply chains. Marit. Econ. Logist. 19, 1–51.

Heredia-Zavoni, E., Montes-Iturrizaga, R., 2019. Modeling directional environmental contours using three dimensional vine copulas. Ocean Eng. 187, 106102.

Herrera, M.P., Gómez-Martín, M.E., R, J., 2017. Hydraulic stability of rock armors in breaking wave conditions. Coast. Eng. 127, 55–67.

Hochstein, A., 1967. A navigation use of industrial canals.

Hoffmans, G.J.C.M., 2012. The Influence of Turbulence on Soil Erosion. Eburon Academic Publishers, Utrecht, the Netherlands.

Joe, H., 1996. Families of m-Variate Distributions with Given Margins and m(m-1)/2 Bivariate Dependence Parameters. Lecture Notes-Monograph Series, vol. 28, pp. 120–141.

Joe, H., 1997. Multivariate Models and Multivariate Dependence Concepts. CRC Press.

Kendall, M.G., 1938. A new measure of rank correlation. Biometrika 30 (1–2), 81–93.

Kindermann, P.E., Antolínez, J.A.Á., Morales-Nápoles, O., 2026. Tail dependence of surge height and wind speed along the dutch coast for storm clusters from large simulated datasets. Nat. Hazards 122, 196.

Kriebel, D., Seelig, W., Judge, C., 1996. Development of a unified description of ship-generated waves. In: Proceedings of the U.S. Section PIANS Annual Meeting, Roundtable and Technical Workshops. PIANC USA, Alezandria, VA, USA.

Lira-Loarca, A., Cobos, M., Losada, M.Á., Baquerizo, A., 2020. Storm characterization and simulation for damage evolution models of maritime structures. Coast. Eng. 156, 103620.

Losada, M.A., Desire, J.M., Alejo, L.M., 1986. Stability of blocks as breakwater armor units. J. Struct. Eng. 112 (11), 2392–2401.

Lucio, D., Lara, J., Tomás, A., Losada, I., 2024. Probabilistic assessment of climate-related impacts and risks in ports. Reliab. Eng. Syst. Saf. 251, 110333.

Lucio, D., Tomás, A., Lara, J., Camus, P., Losada, I., 2020. Stochastic modeling of long-term wave climate based on weather patterns for coastal structures applications. Coast. Eng. 161, 103771.

Luo, Y., Zhao, X., Liu, B., He, S., 2024. Condition-based maintenance policy for systems under dynamic environment. Reliab. Eng. Syst. Saf. 246, 110072.

Mares-Nasarre, P., 2025. Probabilistic estimation of the mean wave overtopping discharge on mound breakwaters. Coast. Eng. 201, 104792.

Mares-Nasarre, P., Argente, G., Gómez-Martín, M.E., Medina, J.R., 2021. Armor damage of overtopped mound breakwaters in depth-limited breaking wave conditions. J. Mar. Sci. Eng. 9 (9).

Mares-Nasarre, P., García-Maribona, J., Mendoza-Luego, M.A., Morales-Nápoles, O., 2023. A copula-based Bayesian network to mdoel wave climate multivariate uncertainty in the Alboran sea. In: Proceedings of 33rd European Safety and Reliability Conference. pp. 1053–1060.

Mares-Nasarre, P., Molines, J., Gómez-Martín, M.E., Medina, J.R., 2022. Hydraulic stability of cube-armored mound breakwaters in depth-limited breaking wave conditions. Ocean Eng. 259.

Mares-Nasarre, P., Morales-Nápoles, O., Hofland, B., Melling, G., 2024a. Armor damage on groins under ship wave attack using field data. In: Proceedings of the 9th Conference on Physical Modelling in Coastal Engineering. Delft (the Netherlands).

Mares-Nasarre, P., Muscalus, A., Haas, K., Morales-Nápoles, O., 2024b. The probabilistic dependence of ship-induced waves is preserved spatially and temporally in the Savannah river (USA). Sci. Rep. 14, 28154.

Mares-Nasarre, P., van Gent, M.R., Morales-Nápoles, O., 2024c. A copula-based model to describe the uncertainty of overtopping variables on mound breakwaters. Coast. Eng. 189, 104483.
Maynord, S., 1996. Return Velocity and Drawdown in Navigable Waterways. Technical Report Hl-96-6, US Army corps of Engineers, Vicksburg, MS, USA.
Van der Meer, J.W., 1988. Rock Slopes and Gravel Beaches Under Wave Attack, vol. 396, Delft hydraulics Delft, Netherlands.
Melby, A., Kobayashi, N., 1999. Damage progression and variability on breakwater trunks. In: Proceedings of Coastal Structures 1999, Balkema, Rotterdam. pp. 309–316.
Melling, G., Jansch, H., Kondziella, B., Uliczka, K., Gätje, B., 2019. Damage to rock groynes from lomg-period ship waves: Towards a probabilistic design method. In: Proceedings of Coastal Structures. pp. 10–19.
Melling, G., Jansch, H., Kondziella, B., Uliczka, K., Gätje, B., 2021. Evaluation of optimised groyne designs in response to long-period ship wave loads at Juelssand in the lower Elbe Estuary. Die Küste 89 (89), 29–56.
Memar, S., Hofland, B., Ragno, E., Melling, G., Morales-Nápoles, O., Nasarre, P.M., Jonkman, S.N., 2025. Probabilistic estimation of primary ship-induced wave heights at estuary groins using a nonparametric Bayesian network. J. Waterw. Port Coast. Ocean. Eng. 151 (4), 04025015.
Mercier, S., Meier-Hirmer, C., Roussignol, M., 2012. Bivariate Gamma wear processes for track geometry modelling, with application to intervention scheduling. Struct. Infrastruct. Eng. 8 (4), 357–366.
Meyers, S.D., Yilmaz, Y., Luther, M.E., 2022. Some methods for addressing errors in static AIS data records. Ocean Eng. 264, 112367.
Molines, J., Bayón, A., Gómez-Martín, M.E., Medina, J.R., 2020. Numerical study of wave forces on crown walls of mound breakwaters with parapets. J. Mar. Sci. Eng. 8 (4).
Morales-Nápoles, O., 2010. Counting vines. In: Dependence Modeling: Vine Copula Handbook. pp. 189–218.
Morales-Nápoles, O., Rajabi-Bahaabadi, M., Torres-Alves, G.A., 't Hart, C.M.P., 2023. Chimera: An atlas of regular vines on up to 8 nodes. Sci. Data 10 (1), 337.
Muscalus, A.C., Haas, K.A., 2022. Vessel wake contributions to erosion at exposed and sheltered shorelines near a tidal shipping channel. Coast. Eng. 178, 104220.
Muscalus, A.C., Haas, K.A., Webster, D.R., 2024. Observations of primary ship waves at the margins of a confined tidal river. J. Waterw. Port Coast. Ocean. Eng. 150 (5), 04024009.
Nelsen, R.B., 2006. An Introduction to Copulas (Springer Series in Statistics). Springer-Verlag, Berlin, Heidelberg.
Nicolai, R.P., Dekker, R., van Noortwijk, J.M., 2007. A comparison of models for measurable deterioration: An application to coatings on steel structures. Reliab. Eng. Syst. Saf. 92 (12), 1635–1650.
Noh, Y., Sun, M., 2025. Environmental contours using copulas for extreme load estimate of offshore wind turbines. Ocean Eng. 326, 120919.
Okafor, E.G., Wang, X., Nafis, B.M., Leda, A., Huitink, D.R., Meng, X., 2023. Reliability evaluation of a novel metal oxide-aluminum glycerol film capacitor using nonlinear degradation modeling with dependency considerations. Qual. Eng. 1–13.
Pan, Z., Balakrishnan, N., 2011. Reliability modeling of degradation of products with multiple performance characteristics based on gamma processes. Reliab. Eng. Syst. Saf. 96 (8), 949–957.
Pugh, D.T., Vassie, J.M., 1978. Extreme sea levels from tide and surge probability. In: Coastal Engineering Proceedings. Vol. 1, p. 52.
Ramousse, B., Mendoza-Lugo, M.A., Rongen, G., Morales-Nápoles, O., 2024. Elicitation of rank correlations with probabilities of concordance: Method and application to building management. Entropy 26 (5).
Romano, A., Bellotti, G., Briganti, R., Franco, L., 2015. Uncertainties in the physical modelling of the wave overtopping over a rubble mound breakwater: The role of the seeding number and of the test duration. Coast. Eng. 103, 15–21.
Rongen, G., Morales-Nápoles, O., Kok, M., 2024. Using the classical model for structured expert judgment to estimate extremes: a case study of discharges in the Meuse river. Hydrol. Earth Syst. Sci. 28 (13), 2831–2848.
Schijf, J.B., 1949. Protection of embankments and bed in inland and maritime waters, and in overflows or weirs. In: Proceedings of XVII International Navigation Congress, Lisbon, Section 1. Lisbon.
Seemann, A., Melling, G., Jansch, H., Kondziella, B., 2023. A design method for rock groynes exposed to overtopping from long-period ship wave loads. J. Coast. Hydraul. Struct. 3.
Sibuya, M., et al., 1960. Bivariate extreme statistics. Ann. Inst. Statist. Math. 11 (2), 195–210.
Singpurwalla, N.D., Wilson, S.P., 1998. Failure models indexed by two scales. Adv. in Appl. Probab. 30 (4), 1058–1072.
Sklar, M., 1959. Fonctions De Repartition a N Dimensions Et Leurs Marges. Vol. 8, Publ. Inst. Statist. Univ. Paris, pp. 229–231.
Spearman, C., 1904. The proof and measurement of association between two things. Am. J. Psychol. 15 (1), 72–101.
't Hart, C.M.P., Morales-Nápoles, O., Jonkman, B., 2024. The influence of spatial variation on the design of foundations of immersed tunnels: Advanced probabilistic analysis. Tunn. Undergr. Space Technol. 147, 105624.
Tajiani, B., Vatn, J., Naseri, M., 2024. Optimizing the maintenance threshold in presence of shocks: A numerical framework for systems with non-monotonic degradation. Reliab. Eng. Syst. Saf. 245, 110039.
USACE, 1984. Shore Protection Manual. U.S. Army Engineer Waterways Experiment Station, Vicksburg, Mississipi.
Valela, C., Nistor, I., Rennie, C.D., Lara, J.L., Maza, M., 2021. Hybrid modeling for design of a novel bridge pier collar for reducing scour. J. Hydraul. Eng. 147 (5).
van Noortwijk, J.M., 2009. A survey of the application of gamma processes in maintenance. Reliab. Eng. Syst. Saf. 94 (1), 2–21, Maintenance Modeling and Application.
Van Noortwijk, J.M., Frangopol, D.M., 2004. Two probabilistic life-cycle maintenance models for deteriorating civil infrastructures. Probabilistic Eng. Mech. 19 (4), 345–359.
Vatter, T., Nagler, T.T., 2022. Pyvinecopulib: A python library for vine copula models. Python package version 0.6.1.
Vidal, C., Losada, M.A., Medina, R., 1991. Stability of mound breakwater's head and trunk. J. Waterw. Port Coast. Ocean. Eng. 117 (6), 570–587.
Vidal, C., Medina, R., Lomónaco, P., 2006. Wave height parameter for damage description of rubble-mound breakwaters. Coast. Eng. 53 (9), 711–722.
Yazdi, M., Khan, F., Abbassi, R., 2022. Operational subsea pipeline assessment affected by multiple defects of microbiologically influenced corrosion. Process. Saf. Environ. Prot. 158, 159–171.
Zhang, J., Hu, C.-H., He, X., Si, X.-S., Liu, Y., Zhou, D.-H., 2017. Lifetime prognostics for deteriorating systems with time-varying random jumps. Reliab. Eng. Syst. Saf. 167, 338–350.
Zhang, J., Huang, X., Fang, Y., Zhou, J., Zhang, H., Li, J., 2016. Optimal inspection-based preventive maintenance policy for three-state mechanical components under competing failure modes. Reliab. Eng. Syst. Saf. 152, 95–103.
Zhang, Y., Kim, C.-W., Beer, M., Dai, H., Soares, C.G., 2018. Modeling multivariate ocean data using asymmetric copulas. Coast. Eng. 135, 91–111.
Zhang, S., Zhou, W., 2014. Cost-based optimal maintenance decisions for corroding natural gas pipelines based on stochastic degradation models. Eng. Struct. 74, 74–85.
Zhao, G., Dong, S., 2025. Long-term extreme responses assessment of a floating offshore wind turbine using mixture distribution models based on C-vine copulas. Ocean Eng. 342, 122813.